Choroideremia Carriers: Dark-Adapted Perimetry and Retinal Structures

Rait Parmann,[1] Vivienne C. Greenstein,[1] Stephen H. Tsang,[1,2] and Janet R. Sparrow[1,2]

[1]Departments of Ophthalmology, Columbia University, New York, NY, United States
[2]Departments of Pathology and Cell Biology, Columbia University, New York, NY, United States

Correspondence: Janet R. Sparrow, Department of Ophthalmology, Columbia University Medical Center, 635 W. 165th Street, New York, NY 10032, USA; jrs88@cumc.columbia.edu.

Received: April 5, 2022
Accepted: June 22, 2022
Published: July 11, 2022

Citation: Parmann R, Greenstein VC, Tsang SH, Sparrow JR. Choroideremia carriers: Dark-adapted perimetry and retinal structures. *Invest Ophthalmol Vis Sci.* 2022;63(8):4. https://doi.org/10.1167/iovs.63.8.4

Purpose. In choroideremia (CHM) carriers, scotopic sensitivity was assessed by dark adapted chromatic perimetry (DACP) and outer retinal structure was evaluated by multimodal imaging.

Methods. Nine carriers (18 eyes) and 13 healthy controls (13 eyes) underwent DACP testing with cyan and red stimuli. Analysis addressed peripapillary (4 test locations closest to the optic disc), macular (52 locations), and peripheral (60 locations outside the macula) regions. Responses were considered to be rod-mediated when cyan relative to red sensitivity was >5 dB. Fundus imaging included spectral domain optical coherence tomography (SD-OCT), short-wavelength (SW-AF), near-infrared (NIR-AF), ultrawide-field (200 degrees) pseudocolor fundus imaging, and quantitative (qAF) fundus autofluorescence.

Results. Detection of the cyan stimulus was rod mediated in essentially all test locations (99.7%). In the macular and peripheral areas, DACP sensitivity values were not significantly different from healthy eyes. In the peripapillary area, sensitivities were significantly decreased ($P < 0.05$). SD-OCT imaging ranged from hyper-reflective lesions and discontinuities of the outer retinal bands to hypertransmission of signal. SW-AF and NIR-AF images presented with peripapillary atrophy in seven patients (14 eyes). Mosaicism was detectable in SW-AF images in seven patients and in NIR-AF images in five patients. Frank hypo-autofluorescence was visible in eight patients with distinct chorioretinopathy in seven patients. The qAF values were below the 95% confidence interval (CI) of healthy age-matched individuals in 12 eyes.

Conclusions. Rod mediated scotopic sensitivity was comparable to that in control eyes in macular and peripheral areas but was decreased in the peripapillary area where changes in retinal structure were also most severe.

Keywords: dark adapted chromatic perimetry, quantitative fundus autofluorescence, near-infrared fundus autofluorescence, optical coherence tomography, retina, short-wavelength fundus autofluorescence

Choroideremia (CHM), an X-linked recessive disorder affecting approximately 1 in 50,000 individuals[1] is caused by mutations in the ubiquitously expressed *CHM* gene (OMIM 300390) encoding Rab escort protein-1 (REP-1) that participates in the lipid modification of Rab GTPases.[2–4] More than 100 disease-causing mutations in CHM have been described. CHM is characterized by progressive degeneration of photoreceptor cells, retinal pigment epithelium (RPE), and the underlying choroid in affected male patients. These individuals can experience slowed dark adaptation and progressive constriction of the visual field but with retained foveal structure and function until the age of 50 to 60 years.[5–9] In affected male patients, spectral domain optical coherence tomography (SD-OCT) imaging has revealed a loss of the interdigitation zone (IZ) and ellipsoid zone (EZ) together with outer nuclear layer (ONL) thinning, and increased signal transmission posterior to RPE/Bruch's membrane. Also noted are outer retinal tubulations and zones of macular sparing that present as islands of autofluorescence (AF).[8,9] The presence of RPE in these islands of preserved retina is signified by a near-infrared fundus autofluorescence (NIR-AF) signal from melanin together with an absence of hypertransmission of the OCT signal into the choroid.[10] Preserved RPE is also associated with better visual acuity.[10] Despite histopathological studies of an affected male patient[11] and carrier female patients[12,13] and the use of high resolution OCT,[1] it has been difficult to determine the sequence of cellular changes leading to vision loss in CHM. The deficiency in REP1 can be offset by REP2 activity in most cell types; however, as evidenced by CHM, compensation is not adequate in the retina.[14,15]

One of the first symptoms of affected male patients with CHM is poor vision in the dark (66% of patients) from a young age; fewer have peripheral field loss (17%) as a primary symptom.[16,17] Some female carriers have no visual disturbances, whereas others report visual function loss, reduced night vision in middle and late life, and abnormal full-field electroretinogram (ERG) recordings.[18–20] In

Investigative Ophthalmology & Visual Science

SD-OCT scans, female carriers can present with hyperreflective lesions in photoreceptor-attributable bands; these lesions interrupt the IZ and EZ hyper-reflectivity layers and correlate with hyperautofluorescent foci visible in the macula.[8,19] In short wavelength fundus autofluorescence (SW-AF) images acquired from CHM carriers, a mosaic is created by patches of relatively higher and lower autofluorescence intensities.[10,19,21,22] Moreover, we have observed that the areas of reduced SW-AF in the mosaic correspond to NIR-AF originating in melanin.[10] It has been suggested that non-uniform melanin distribution associated with CHM/REP-1 dysfunction could represent an X-linked manifestation of altered RPE melanosome transport in affected males and female carriers.[23] However, we have also studied melanin pigment mosaicism (NIR-AF) in carriers of X-linked albinism (GPR143/OA1) and, unlike in CHM carriers, patches of reduced signal in NIR-AF images of GPR143/OA1 carriers co-localize with increased signal (not reduced signal) in SW-AF images.[24] SW-AF measured as quantitative fundus autofluorescence (qAF) is profoundly reduced not only in CHM affected patients but also in female CHM carriers.[10]

Our aim here was to assess night vision problems in CHM carriers by measuring rod sensitivity.[25,26] Thus, we recorded dark-adapted visual field sensitivities in CHM carriers and compared these findings to structural features of the retina as assessed by multimodal imaging.

Methods

Subjects

This was a cross-sectional study of nine CHM carriers (18 eyes). All patients were enrolled under the protocol #AAAR8220 approved by the Columbia University Medical Center Institutional Review Board. All procedures adhered to tenets set out in the Declaration of Helsinki. Each patient included in the study underwent a complete ophthalmic examination by a retinal specialist (author S.H.T.) including slit-lamp examination, dilated fundus examination, and measurement of best-corrected visual acuity (BCVA). All patients were diagnosed as CHM carriers either by genetic sequencing or by clinical findings and family history.

Pupils were dilated with topical 1% tropicamide and 2.5% phenylephrine. Clinical data for all patients were obtained during the same visit and included dark-adapted chromatic perimetry (DACP), SD-OCT scans, three modalities of fundus autofluorescence – SW-AF, NIR-AF, and qAF; and ultrawide-field fundus photographs.

Dark-Adapted Chromatic Perimetry

Dark-adapted visual fields were measured with a dark-adapted chromatic perimeter (Medmont International Pty Ltd., Victoria, Australia). Patients were dark-adapted for 40 minutes before testing. A 1.73 degree stimulus was presented for 200 ms. The response time was 1100 ms and the time between stimuli was set at 400 ms. Scotopic sensitivities were first tested to a cyan stimulus (505 nm) and then to a red stimulus (625 nm). The cyan stimulus (dominant wavelength = 505 nm and half bandwidth = 28 nm) had a maximum luminance of 12.58 cd/m^2 and a dynamic range of approximately 75 dB. The maximum luminance of the red stimulus (dominant wavelength = 625 nm and half bandwidth = 25 nm) was 4.64 cd/m^2 with an approximately 50 dB dynamic range. The grid had 112 test locations that extended 120 degrees across the nasal to temporal field and 78 degrees superior to inferior. Brightness of the fixation light was set to a minimum level still visible to a patient and the correct alignment of the pupil was observed throughout the test by the inbuilt infrared camera. To determine whether the response at each locus is mediated by the rod or cone system, or a mixture of them, the principle of two color dark-adapted perimetry can be used (i.e. sensitivity to a cyan stimulus is compared to sensitivity to a red stimulus at the same location).[27–29] As previously described,[28] loci were considered as rod-mediated when the spectral sensitivity difference (SSD; cyan-red) at a given point was >5 dB. For better evaluation, three separate areas, peripheral, macular, and peripapillary, were used to assess the sensitivity of the carriers in relation to the normal controls (Fig. 1E). The mean and median values were calculated for all loci in each of the three areas. The macular area consisted of test points extending from the fovea horizontally and vertically with a radius of 18 degrees (52 locations). Inside that area, additional attention was given to the peripapillary area, defined by four test points closest to the blind spot with the following coordinates (x and y) relative to the position of the fovea (coordinates 0 degrees, 0 degrees): 12 degrees, 0 degrees; 18 degrees, 0 degrees; 12 degrees, 4 degrees; 12 degrees, and −4 degrees. The peripheral area included all other test points outside the 18 degrees macular area (60 locations). For control data, the dominant eyes of 13 healthy subjects were tested using the same protocol. The control group had a mean age of 34 years (range = 23–48 years) and consisted of 7 women and 6 men. All had visual acuity of 20/20 or better and no evidence of any eye disease or high refractive error (+/−6.00 DS) on ophthalmologic examination at the time of testing. The horizontal visual field axis was transposed when necessary to make all eyes the right eyes for statistical analysis. An unequal variance two-sample *t*-test was used to compare sensitivity values for the two groups.

Humphrey Visual Field

In one case (P9, both eyes) automated "white on white" 30-2 visual field (VF) tests (Humphrey Field Analyzer 3; Carl Zeiss Meditec, Dublin, CA, USA) were obtained using the Swedish Interactive Threshold Algorithm (SITA) fast technique.

Fundus Imaging

SD-OCT line and volume scans (870 nm, 30 degrees × 30 degrees field and 55 degrees × 55 degrees field) were acquired in high-resolution mode with a corresponding infrared reflectance fundus image (820 nm) using a confocal scanning laser ophthalmoscope (Spectralis HRA+OCT; Heidelberg Engineering, Heidelberg, Germany). Using the Spectralis SW-AF (488-nm excitation, 500-nm barrier filter; 30 degrees × 30 degrees field and 55 degrees × 55 degrees field) and NIR-AF images (787 nm excitation, >830 nm emission; 30 degrees × 30 degrees field) were also acquired using automatic real-time tracking and 100 single frames were averaged and saved in the normalized mode.

The methods for acquisition of images for qAF have previously been described.[30–34] Briefly, following pupil dilatation, SW-AF images (480 nm excitation, 30 degrees × 30 degrees) were acquired using a Spectralis HRA+OCT equipped with an internal fluorescent reference for correction of variable laser power and differences in detector

Investigative Ophthalmology & Visual Science

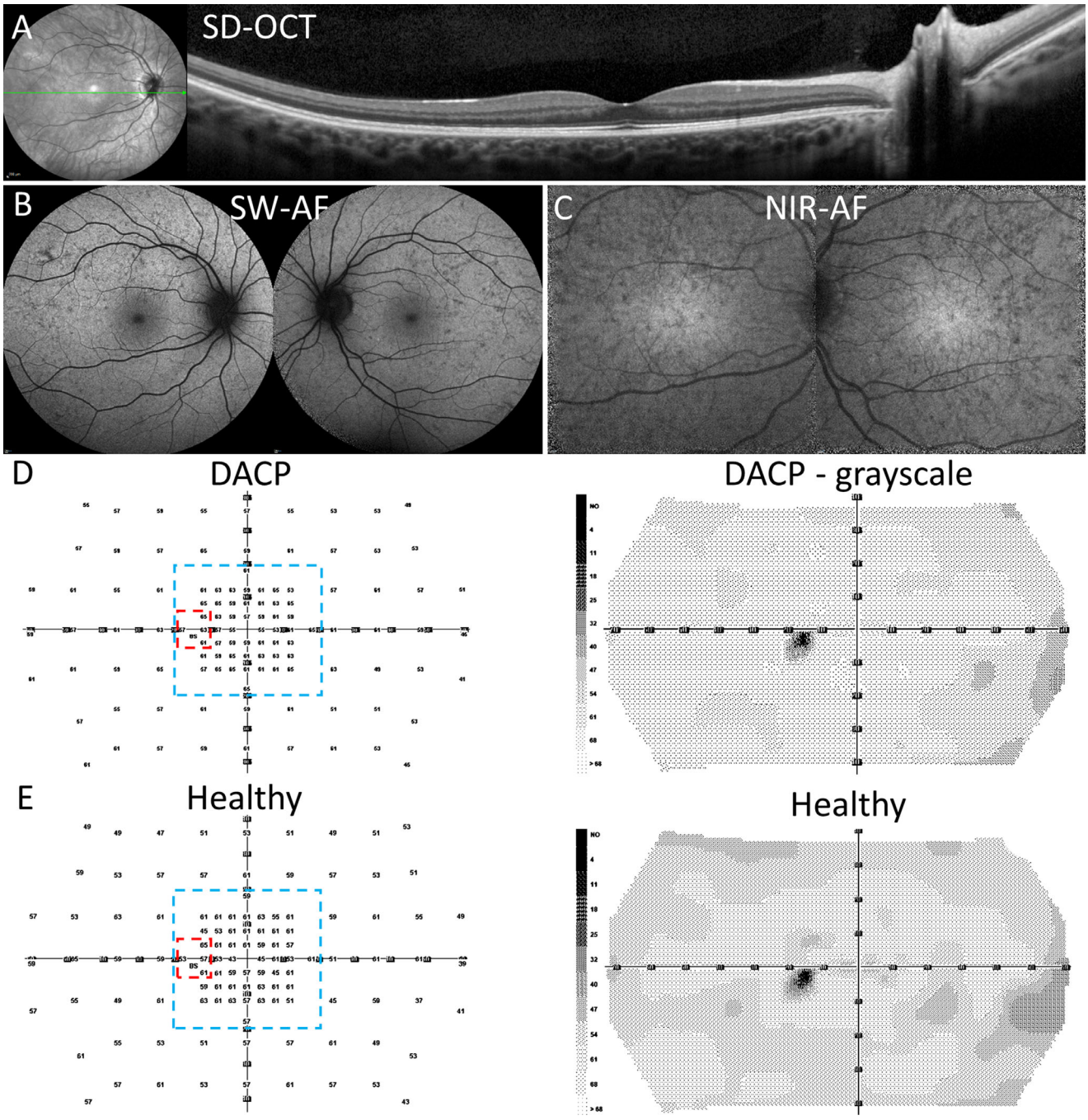

Figure 1. Multimodal images and dark-adapted chromatic perimetry (DACP. P7. (**A**) Spectral domain optical coherence tomography (SD-OCT) horizontal scan through the fovea demonstrating normal retinal structure. The axis of the scan is shown as the green line in the near-infrared reflectance image on the left. (**B**) Short-wavelength autofluorescence (SW-AF) showing dispersed hypo-autofluorescent foci. (**C**) Near-infrared autofluorescence (NIR-AF) exhibiting a mosaic of relative hypo- and hyperautofluorescence and preserved central hyperautofluorescence. (**D**) DACP acquired from P7 (OS). A cyan field presents as a numeric grid with sensitivity values in dBs and grayscale map. Areas outlined by dashed lines are the sub-regions used for visual field analyses; red marks the peripapillary area and blue the macular area. (**E**) DACP cyan field numeric and grayscale map of a healthy left eye.

sensitivity. The images were acquired in the high-speed mode (8.9 frames/second), as a minimum of 12 frames (video format). For image analysis, grey levels were calibrated to the internal fluorescence reference, ocular media absorption, and refraction. For all eyes, color-coded qAF images were generated based on pixel-wise transformation of qAF values (WaveMetrics, Lake Oswego, OR, USA). Comparison was made to healthy controls of similar age without eye disease and as described by Greenberg et al.[35]

Ultrawide-field (200 degrees) pseudocolor fundus images (lasers: red, 633 nm; green, 532 nm; with red and green false-color display) and fundus autofluorescence images

Investigative Ophthalmology & Visual Science

(532 nm excitation) were also obtained using an Optos Daytona (Optos plc, Dunfermline, Scotland, UK).

Statistical Analysis

Statistical analyses were performed using Microsoft Office Excel Analysis ToolPak (Microsoft, Redmond, WA, USA) and GraphPad Prism software (GraphPad Software, San Diego, CA, USA). The latter was also used for the creation of scatter plots. For *P* value calculations Welch's *t*-test (unequal variances *t*-test) was used.

Results

Demographics

Nine (9) female CHM carriers (18 eyes) were analyzed in this study; the mean age was 42.3 +/− 10.2 years (age range = 19.3–57.4). Cohort demographics and genetic results are presented in the Table. Four patients (P4 and P3, the mother and her daughter; P8; P9) were not genetically screened but were clinically diagnosed on the basis of frank hypo-autofluorescent changes in SW-AF, changes in outer retinal layers, and hyper-reflective lesions in SD-OCT. These four patients also demonstrated positive family histories of CHM. Specifically, P4 (the mother of P3) has a father and a son with genetically confirmed CHM. P8 has a father and a paternal uncle with genetically confirmed CHM. P9 has a son with genetically confirmed CHM. Overall, eight of nine patients reported a family history consistent with X-linked inheritance. Only P6 did not have a known family history (although the patient's son reported night vision issues). Seven (7) of nine (9) patients presented with symptoms that can be associated with CHM carrier status: some level of night blindness or impaired dark adaptation, photosensitivity, and peripheral vision disturbances. In one case (P8), the symptoms were present from childhood; all other symptomatic subjects reported a history of 1 to 5 years. P3 and P7 (the 2 youngest in the cohort, 19.3 and 36.9 years, respectively) did not report any visual problems. Fundus examination revealed varying levels of retinal involvement in all patients ranging from eyes having a symmetrical appearance (P6 and P7) to completely asymmetrical presentations (P8 and P9). On fundoscopy, seven patients presented with chorioretinal atrophy, occurring mainly around the optic disc and exhibiting inter-eye asymmetry. In P6 and P7, chorioretinal atrophy was not observed.

Fundus Imaging

SD-OCT scans revealed that eight patients out of nine (16 eyes) exhibited at least some level of change in retina. By using the 55-degree scans, the fundus was evaluated not only in the macula but in the midperiphery as well. Changes were not limited to a specific area of the retina but were scattered over the scanned region. No changes were present in the retina of P7 (see Fig. 1A); P3 exhibited mild changes consisting of attenuation of the external limiting membrane (ELM), EZ and IZ bands; hyper-reflective lesions were observed in photoreceptor-attributable bands. The latter carriers were the youngest and only individuals reporting no symptoms. Two patients (P5 and P6) had moderate findings of hyper-reflective lesions (Fig. 2A, P5) and discontinuity of the outer retinal bands. The remaining members of the cohort (P1, P2, P4, P8, and P9) presented with more severe findings that included peripapillary atrophy and additional areas of atrophy in the macula; also observed were hyper-reflective foci that interrupted the photoreceptor-attributable OCT bands and extended into the ONL. Hypertransmission of SD-OCT signal was present in the peripapillary area of both eyes in P1, P2- and P5 (see Figs. 2A [P5], 2D [P2], 3A [P1]). In some cases, photoreceptor-attributable bands were disrupted or absent (see Figs. 2D [P2], 3A [P1]). In P1, the area of peripapillary atrophy presented with a mostly absent outer retina, an outer retina tubulation, inner nuclear layer subsidence, and choroidal thinning.

All patients had widespread changes in the SW-AF images. Mosaics of patches of relative hyperautofluorescence alternating with patches of hypo-autofluorescence (see Fig. 2B, magnified area) were visible in images acquired from P1, P2, P4, P5, P7, and P9, with P7 exhibiting somewhat milder involvement (see Fig. 1B). Frank hypo-autofluorescence indicative of large areas of atrophy was also observed in P3 to P6 and P9 (see Figs. 2B, 4B). In some cases (P1, P2, and P8), only limited islands of spared tissue persisted (see Fig. 3B). As seen in fundoscopy, hypo-autofluorescent atrophic areas surrounded 14 out of 18 optic discs and varied from small areas encircling the disc (P5) to widespread atrophy extending through the macula and periphery (P1 and P8). Interestingly, P1 and P2 were carriers who exhibited hyperautofluorescent dots surrounding

Table. Patient Demographic, Clinical, Genetic, and DACP Data

								DACP Cyan Test Sensitivity (dB)			
								Mean		Median	
			BCVA (logMar)		Spherical Equivalent (D)			OD	OS	OD	OS
ID	Age, y	Race	OD	OS	OD	OS	CHM Variant	Periphery/Macular/Peripapillary			
1	38	African American	0.5	0.4	1.38	0.75	c.1584_1587del p. (Val529Hisfs*7)	40/43/27	48/51/36	41/45/27	49/53/33
2	49	Caucasian	0	0.1	−0.63	−0.63	c.49+3A>G (Intronic)	53/53/47	51/54/49	53/54/46	51/56/51
3	19	Caucasian	0	0	0.25	0.25	–	57/58/47	59/58/42	59/59/47	59/61/40
4	50	Caucasian	0.3	0.1	3.0	1.5	–	55/58/43	48/50/44	55/59/44	48/51/45
5	44	Caucasian	0	0	−0.75	0.25	c.757C>T p. (Arg253*)	56/59/50	52/56/45	57/61/49	55/57/45
6	47	Caucasian	0	0	1.13	1.38	c.1584_1587del p. (Val529Hisfs*7)	60/60/51	59/60/56	61/61/49	61/61/57
7	37	Caucasian	−0.1	−0.1	−0.38	−0.25	c.877C>T p. (Arg293Ter)	60/62/59	57/61/62	61/61/61	57/61/62
8	40	Caucasian	0	0	1.25	1.38	Deletion of the entire gene*	56/59/55	54/59/45	57/61/60	55/61/44
9	57	Caucasian	0.1	0.1	0.63	2.38	c.189G>C p. (Gln63His)†	53/59/50	49/49/47	53/60/47	49/50/49

BCVA, best corrected visual acuity; DACP, dark-adapted chromatic perimetry.
* Results from the patient's paternal uncle, the patient's father also has a confirmed CHM diagnosis.
† Results from the patient's son.

Investigative Ophthalmology & Visual Science

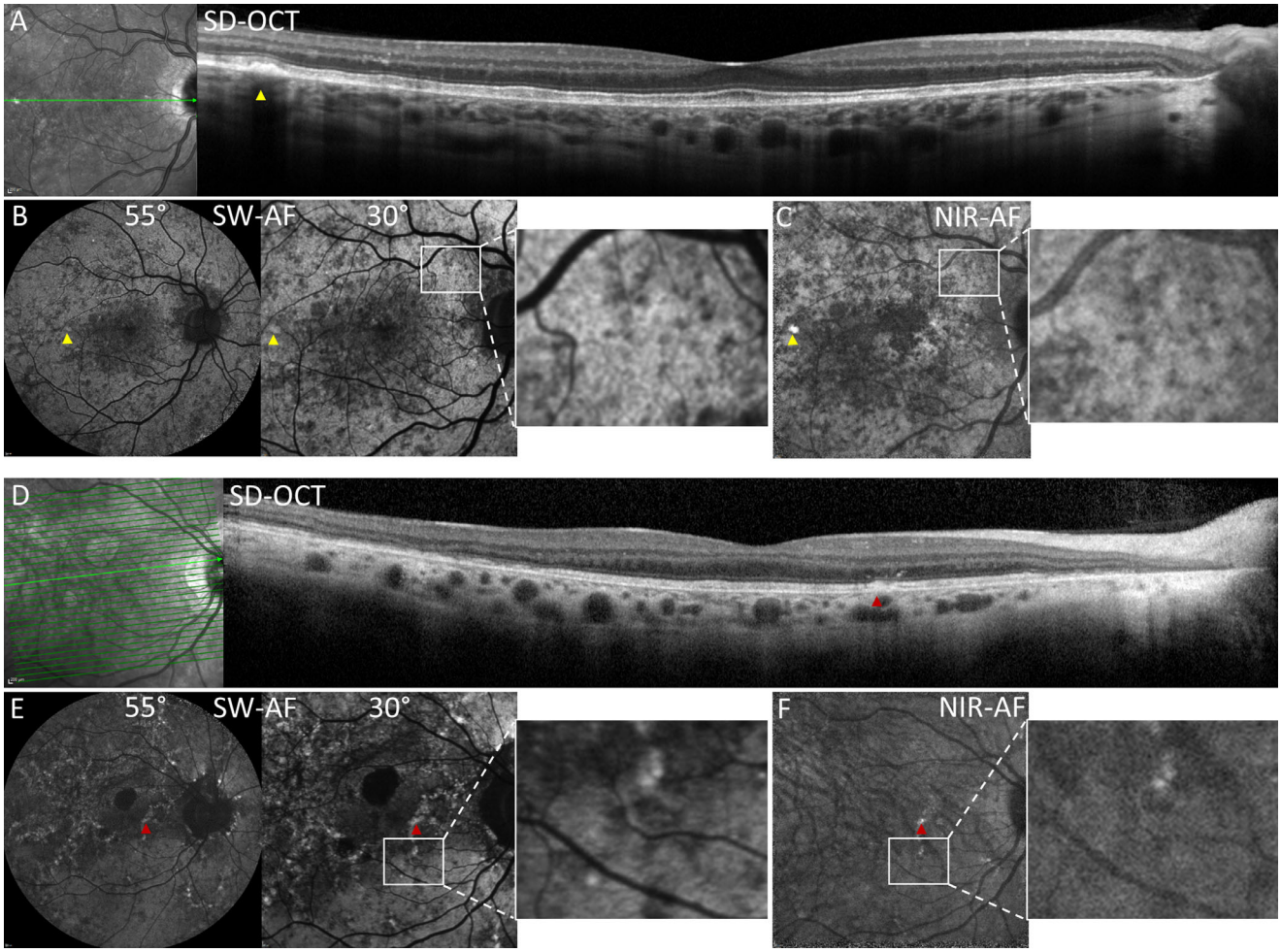

Figure 2. Multimodal images of CHM carriers. P5 (**A–C**) and P2 (**D–F**). (**A**) SD-OCT scan. A hyper-reflective lesion (*yellow arrowhead*) displaces the ellipsoid zone (EZ) band and external limiting membrane (ELM) and corresponds spatially to hyperautofluorescent foci in **B** and **C** (*yellow arrows*). The axis of the horizontal scan is shown as the *green line* in the near-infrared reflectance image on the left. (**B**) SW-AF images (30 degrees and 55 degrees) present central hypoautofluorescence surrounded by a patchwork of hyper- and hypo-autofluorescence. The *white rectangles* outline an area featuring hypo-autofluorescent and hyperautofluorescence patches that spatially correspond in SW-AF (**B**) and NIR-AF (**C**) images. (**C**) NIR-AF image reveals abnormal central hypo-autofluorescence, the mosaic of hypo-autofluorescence and hyperautofluorescence (*white rectangle*), and a hyperautofluorescent spot (*yellow arrowhead*). (**D**) SD-OCT scan reveals a hyper-reflective lesion extending through EZ band (*red arrow*) that corresponds spatially to hyperautofluorescent foci in **E** and **F** (*red arrows*). EZ and ELM are disrupted temporally, and photoreceptor-attributable reflectivity bands are absent in the peripapillary zone. Hypertransmission of signal is visible nasally and choroidal vessels are enlarged. The axis of the horizontal scan is shown as the *green line* in the near-infrared reflectance image on the left. (**E**) SW-AF images (30 degrees and 55 degrees) demonstrate hyperautofluorescent speckles, a mosaicism of hypo- and hyperautofluorescence (*white rectangle*) and peripapillary and macular atrophy presenting as larger areas of hypo-autofluorescence. (**F**) NIR-AF image displays a mosaic of hypo- and hyperautofluorescence (*white rectangle*). The normal hyperautofluorescence of the foveal region is lost.

dark hypoautofluorescent lesions (see Figs. 2E, 3B, 3C); in P1, these speckles were only present in the NIR-AF image, whereas in P2, the speckles were only present in the SW-AF image. Also unexplained in the case of P1, was peripapillary atrophy having reduced SW-AF signal but unchanged or brighter NIR-AF signal (see Figs. 3B, 3C).

SW-AF was measured by qAF using non-normalized SW-AF images. For each patient, qAF levels were calculated as the mean of intensities determined in each 8 circularly arranged segments situated at an eccentricity of 7 to 9 degrees relative to the fovea. The values were calculated for right and left eyes separately because of the asymmetrical nature of the condition. The qAF was plotted versus age and compared with the 95% confidence intervals (95% CIs) of healthy eyes. The qAF values for CHM carriers were below or within the lower limits (Fig. 5) of 95% CI when compared with healthy subjects with one exception: qAF values for P7 were similar to the mean values of age matched control eyes. Nevertheless, the qAF color-coded image differed from a healthy color-coded image and is a good example of mosaicism (see Figs. 1, 5). In four patients, qAF values differed markedly between eyes further confirming the asymmetrical presentation of CHM carrier status. On the whole, qAF color maps corroborated the calculated qAF values, there being an overall decrease in qAF except in the case of P7. These results are consistent with our previous observations.[10]

NIR-AF images revealed mosaicism in carriers P1, P4, P5, P7, and P9 with the patches of reduced autofluorescence in SW-AF corresponding to patches of reduced AF in NIR-AF

Investigative Ophthalmology & Visual Science

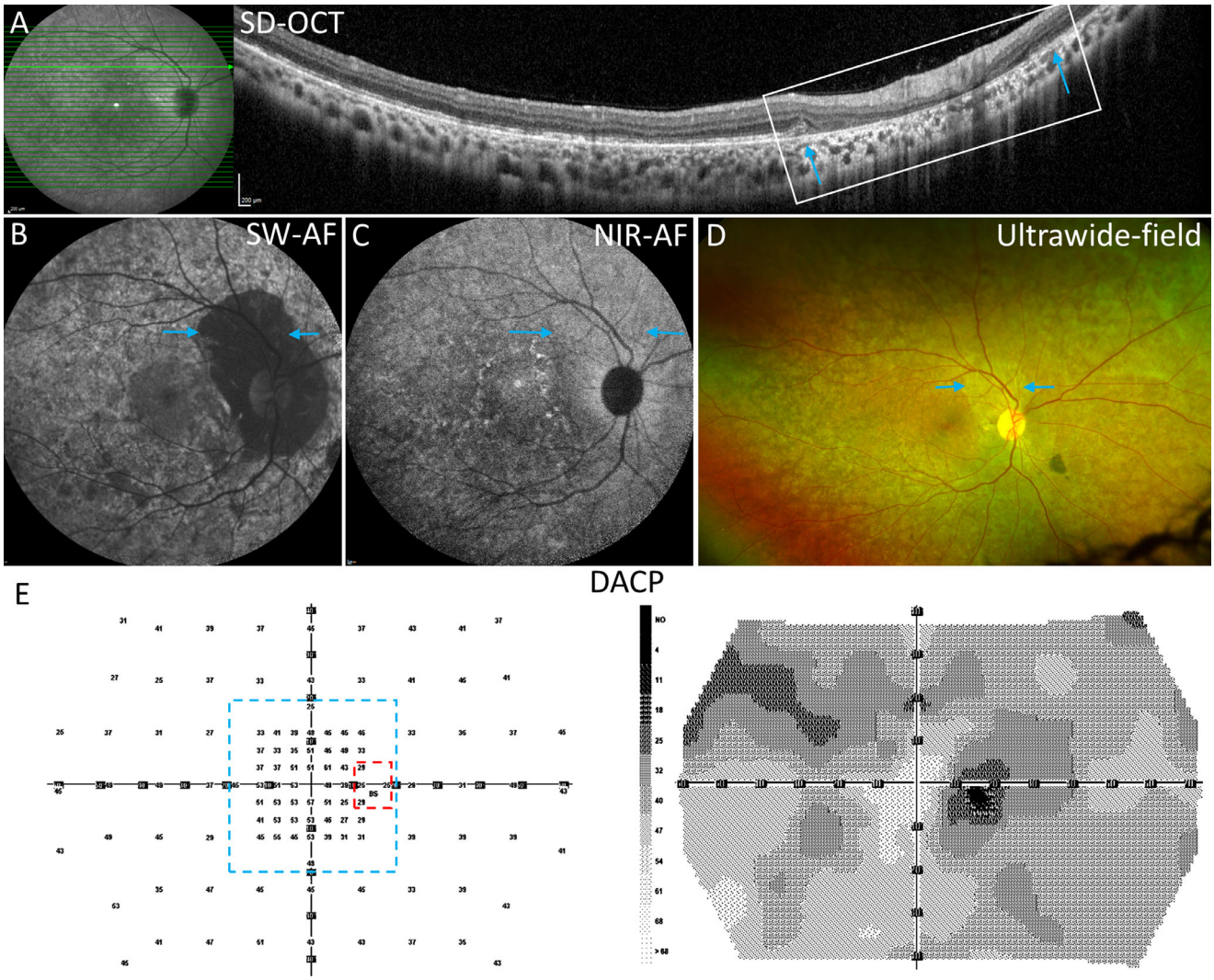

Figure 3. Multimodal images and dark-adapted chromatic perimetry (DACP) P1. (**A**) SD-OCT scan through the zone of peripapillary atrophy. EZ band disruption is apparent temporally. Peripapillary zone is marked by outer retinal loss and hypertransmission of signal (*white rectangle*). The margins of atrophy (*blue arrows*) in the SD-OCT scan correspond spatially to the positions marked by blue arrows in **B** to **D**. The axis of the horizontal scan is shown as the *green line* in the near-infrared reflectance image on the left. (**B**) The SW-AF image reveals a mosaic of hypo- and hyperautofluorescence, extensive mottling, widespread peripapillary atrophy, and faint hyperautofluorescent speckles. (**C**) The NIR-AF shows a mosaic of hypo- and hyperautofluorescence patches, and perifoveal hyperautofluorescent speckles. (**D**) Ultrawide-field image reveals mosaicism in the peripheral retina. (**E**) DACP cyan field- numeric grid and grayscale map. The *dashed lines* indicate the subregions used for visual field analyses: *red*, the peripapillary area; and *blue*, the macular area.

(see Figs. 1C, 2C, 3C). In P2, the mosaicism was less apparent perhaps because of more extensive atrophy. P7 (OU) was the only carrier that retained the normal hyperautofluorescence characteristic of the fovea and parafovea in NIR-AF images (see Fig. 1C). In P5, hyperautofluorescent puncta in the SW-AF images corresponded spatially to hyperautofluorescent foci in NIR-AF images (see Figs. 2B, 2C, magnified areas). This included the peripapillary atrophy. However, in P1, the dark peripapillary atrophy in the SW-AF image appeared to be of normal intensity in the NIR-AF image (see Figs. 3B, 3C).

Dark Adapted Chromatic Perimetry

Dark adapted cyan and red visual fields were obtained from all participants. The reliability factor (% of false positive responses) stayed below the acceptable 20% threshold for all participants, being on average 6.6% ± 4.8 SD (range = 0–17.6%) for cyan and 4.3% ± 3.9 SD (range = 0–18.8%) for the red stimulus. The duration for the cyan test averaged 22.1 minutes ± 1.8 SD (range = 19.4–25.9 minutes) and for the red 23.4 minutes ± 4.7 SD (range = 18.8–37.5 minutes). To assess whether rods or cones mediated detection at each location, we determined the spectral sensitivity difference (SDD; cyan – red) at each point. As previously described,[28] loci were designated as rod-mediated when the SDD was >5 dB. For virtually all test locations (99.7%), the differences calculated as cyan – red were greater than 5 dB, indicating that they were rod-mediated. Thus, only cyan values are plotted in Figure 6. Three separate areas, peripheral, macular, and peripapillary, were used to evaluate the sensitivity of carrier eyes in relation to normal control eyes. The analysis included both eyes from all CHM carriers in comparison to only one eye from each control because of the observed asymmetrical presentation in carriers. Rod-mediated

Investigative Ophthalmology & Visual Science

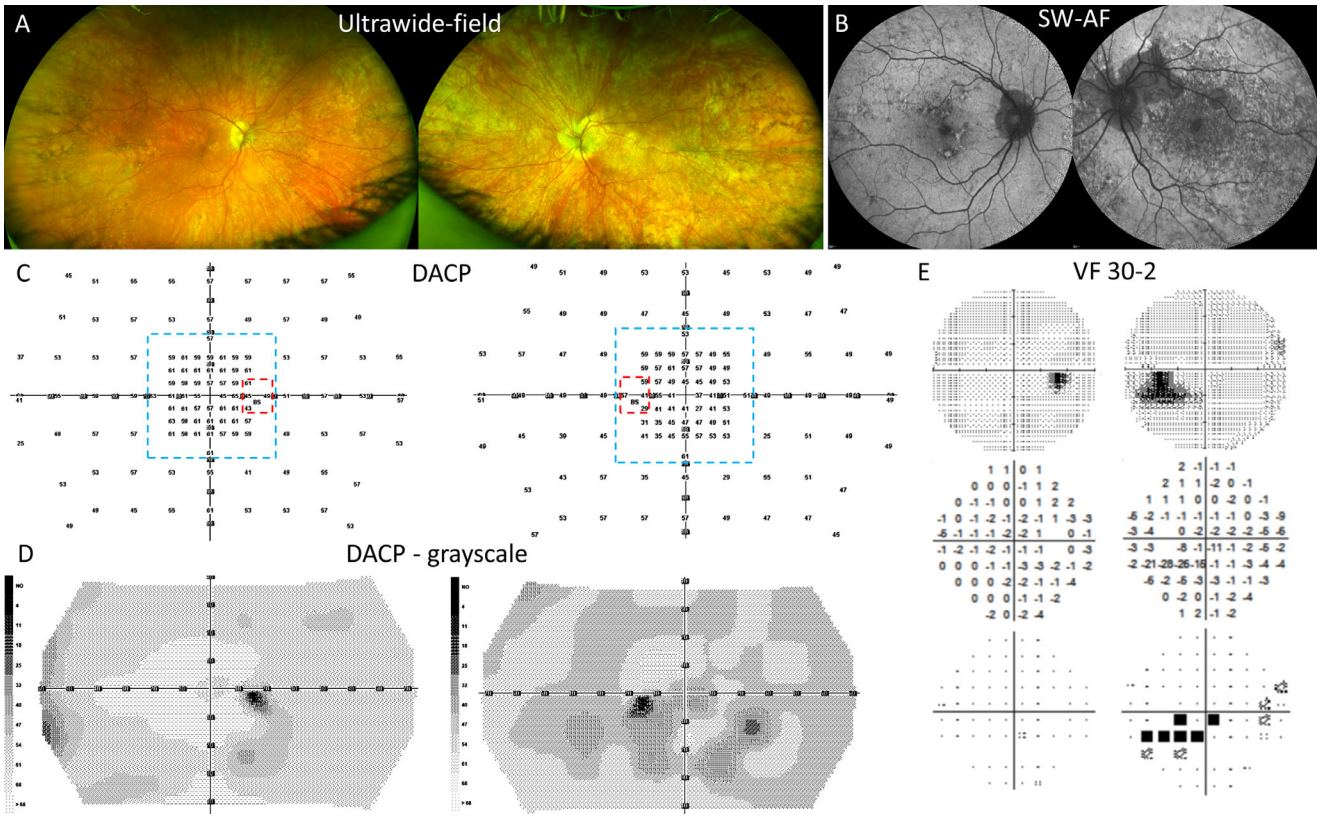

Figure 4. Multimodal images and dark-adapted chromatic perimetry (DACP) reveal asymmetry between the eyes P9. (**A**) Ultrawide-field images demonstrating pigmentary changes overlaying all visible retina (OS > OD). (**B**) SW-AF images demonstrate the asymmetry in terms of atrophy and autofluorescence mosaicism. (**C**) DACP cyan field numeric grid for right and left eyes with values in dBs. Areas delimited by *dashed lines* are the subregions used for sensitivity analyses: *red* marks the peripapillary area; and *blue* marks the macular area. (**D**) DACP grayscale map illustrating the asymmetry of scotopic sensitivity between the right and the left eyes. (**E**) The 30-2 visual fields for right and left eyes: grayscale, total deviation, and probability plots. The results for the right eye test are within normal limits. The grayscale plot for the left eye shows an enlarged blind spot (BS) and a scotoma below the BS which correlates spatially with the atrophy superior to the optic disc visible in panel **B**.

sensitivity data from healthy control eyes (Supplementary Table S1) and CHM carriers are shown in Figure 6 in the form of scatter plots of the median values for each tested eye. For the three areas (macular, peripapillary, and peripheral), with the exception of one outlier in the peripheral area, results from the control eyes are relatively uniform and are within or close to the interquartile (first and third quartile) range. For the CHM carriers, the median values are more spread out reflecting the different state of involvement of retina. In the macular area, the collective median value is similar between the two groups. However, the interquartile range is larger in the carrier group, and three carrier eyes (P1 OD, P4 OS, and P9 OS) have values below the first quartile. The latter all have changes in retinal structure and all three patients reported night vision complaints. For the peripapillary area, the median values and interquartile range are decreased compared with the controls. Three carrier eyes (P1 OU and P3 OS) have markedly decreased median values, values below the first quartile. The difference between the median values of carrier and control eyes is statistically significant ($P < 0.05$, Welch's *t*-test). This finding is consistent with the observed peripapillary atrophy. For the peripheral area, the median value in the CHM carrier group is slightly higher than the median value of controls. However, the interquartile range is clearly wider in the carrier group, and sensitivity values for 4 eyes (P1 OU, P4 OS, and P9 OS) are below the first quartile. Median and mean values for all CHM carriers for all three areas are presented in the Table. To evaluate the inter-eye cyan sensitivity differences in each patient, we calculated the corresponding *P* values for peripheral and macular areas (we did not perform the calculations for the peripapillary areas because of the small number of test points in this region). For the peripheral area, the differences were statistically significant between the eyes ($P < 0.05$) for the following patients: P1, P4, P7, and P9; for the macular area the differences were statistically significant for P1, P4, and P9 ($P < 0.05$).

P1 demonstrated the greatest decreases in DACP sensitivities of the 9 participants. The cyan field for the right eye showed markedly decreased sensitivities (median value 27 dB) in the peripapillary area. Median values for the macula and periphery (45 dB and 41 dB, respectively) were also clearly below the first quartile within the CHM carrier groups. The regions of decreased sensitivity can be seen in the DACP grayscale map for the right eye (see Fig. 3E); the lower sensitivity is represented by the dark gray areas around the blind spot and in the superior field. These functional findings are consistent with the results from imaging modalities. The SW-AF image for P1 (see Fig. 3B) shows an extensive hypo-AF area surrounding the optic disc, and there is atrophy of the outer retinal layers on the SD-OCT scan (see

Investigative Ophthalmology & Visual Science

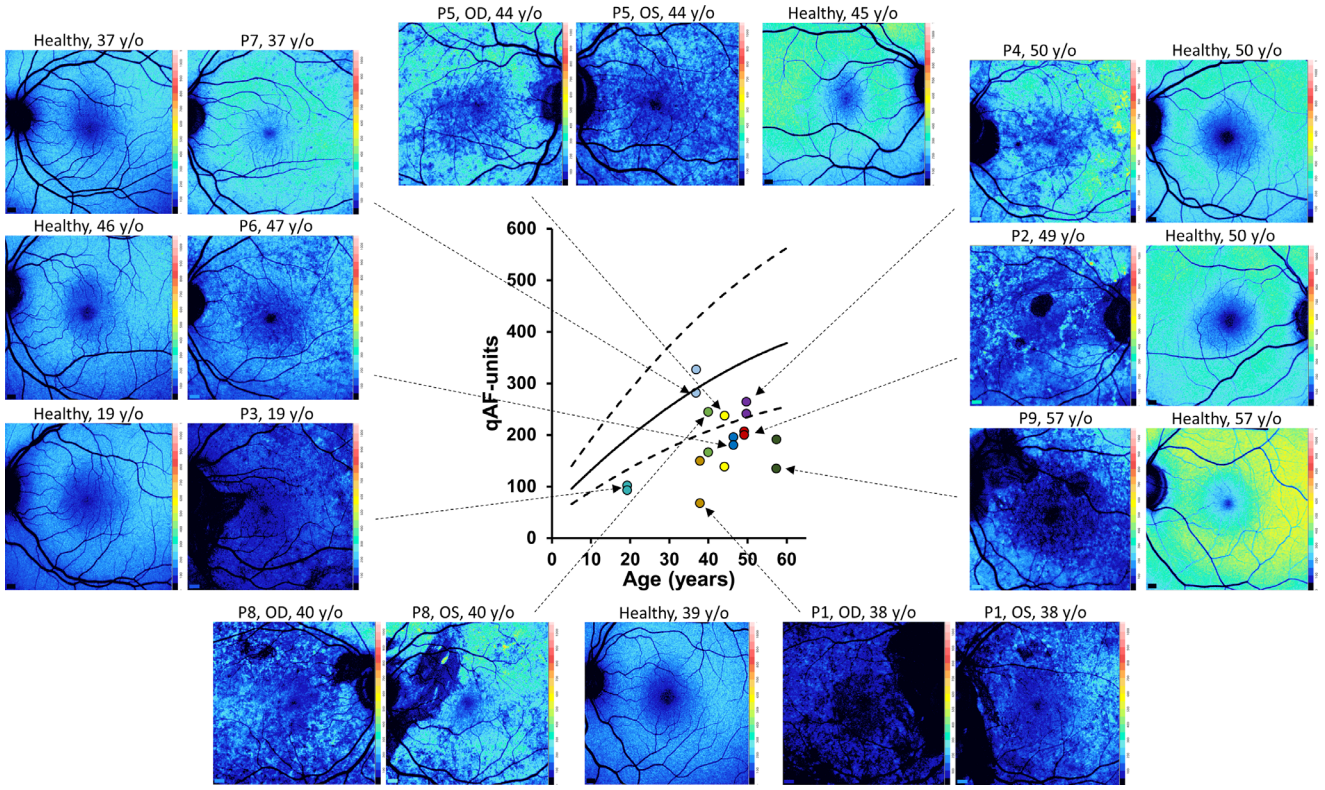

Figure 5. Quantitative fundus autofluorescence (qAF). The qAF values acquired from eight concentric segments (7 to 9 degrees eccentricity) are plotted as a function of age for choroideremia carriers (*symbols*) together with mean and 95% confidence intervals (*black solid and dashed lines*) for healthy control eyes. The qAF color-coded images acquired from the carriers are also presented along with images from age-similar controls.

Fig. 3A). In addition, the qAF color-coded image exhibits a relatively good spatial correlation with the DACP grayscale map. Indeed, the qAF value is significantly decreased and the lowest of the CHM carriers (see Fig. 5). In addition to one mutation in the CHM gene, P1 had a likely pathogenic mutation in *CDHR1* (c.55+1G>A [Splice donor]) and in multiple other genes (8 genes with 8 variants, all of uncertain significance). The *CDHR1* gene is associated with autosomal recessive cone rod dystrophy and retinitis pigmentosa.[36,37]

A good example of DACP inter-eye asymmetry and regional variability is represented by P9. The median scotopic sensitivity values for the macular area are 60 dB for the right eye and 50 dB for the left eye with the left eye value being clearly decreased compared with the control eyes. Visually this can be easily appreciated in the DACP grayscale maps (see Fig. 4D). Although there is a marked difference in the extent of peripapillary changes in SW-AF images (see Fig. 4B, OS > OD), the same was not seen in the analysis of peripapillary sensitivity (the area consists of 4 test locations around the optic disc which make the results dependent on the shape of the peripapillary atrophy). P9 was the only subject who had an automated 30-2 visual field test (no fixation losses and false-positive response $\leq$4% indicating good reliability). The results acquired for the left eye revealed decreased sensitivities for test locations around and inferior to the blind spot which spatially correlates to the peripapillary atrophic area in SW-AF image. The median values for DACP peripheral areas were 53 dB for the right eye and 49 dB for the left eye; the difference was statistically significant ($P = 0.0005$). Grayscale maps for the same area reveal large areas exhibiting an irregular pattern of decreased sensitivity in the left eye whereas the right eye has only minor changes.

Discussion

The findings in this study reveal that rod sensitivities measured by DACP in our group of CHM carriers were not significantly different from those for controls in the macular and peripheral areas but were significantly lower in the peripapillary region. We tested both eyes in CHM carriers and observed DACP inter-eye asymmetry as was also the case when fundus images and qAF were examined.

The DAC perimeter can be used to quantify rod function at individual locations across the visual field[28] making it potentially suitable for evaluating mosaic patterns of retinal dysfunction. It has been evaluated in clinical studies for test-retest repeatability in healthy eyes, age-related degeneration, and inherited retinal degenerations, and results have been found to be within an acceptable level and comparable to those from other perimetry devices.[38,39] As noted above, DACP sensitivities for our group of CHM carrier eyes were not significantly different from those of controls in the macular and peripheral areas. The only statistically significant difference between the groups was in the peripapillary area, a small region consisting of four test points closest to the optic disc. This finding is consistent with an interesting observation that 14 of the 18 eyes had peripapillary atrophy. Peripapillary atrophy has been described in other studies as well.[21,40] None of the eyes in our cohort were highly

Investigative Ophthalmology & Visual Science

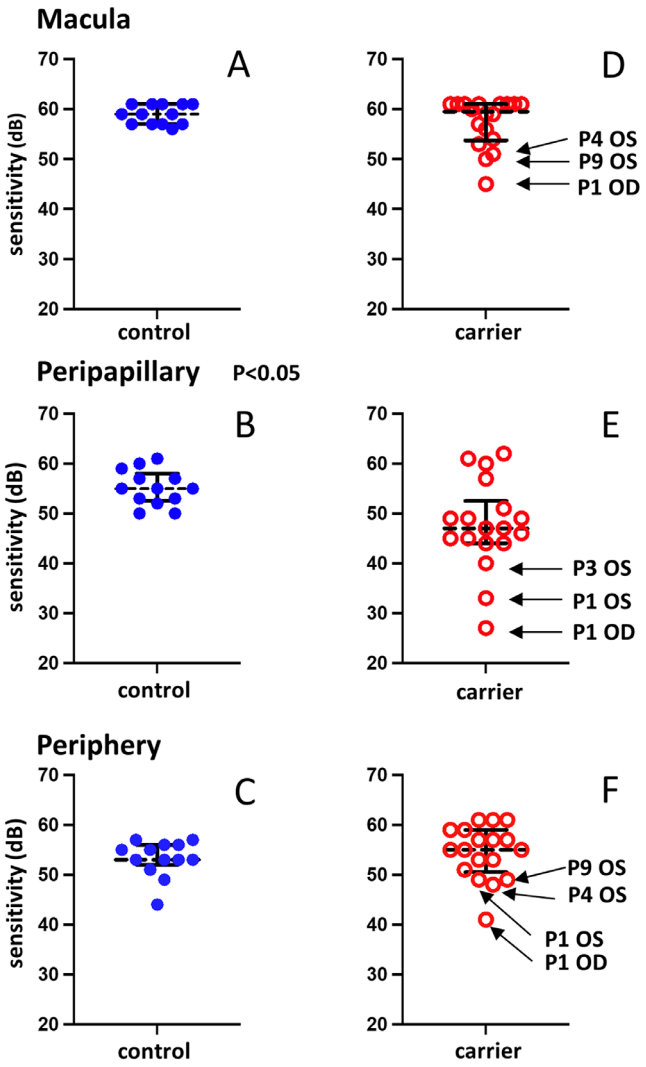

Figure 6. Dark-adapted chromatic perimetry (DACP) results acquired from nine choroideremia carriers and healthy control eyes. Sensitivities to a cyan stimulus (505 nm) are plotted for the macular, peripapillary, and peripheral locations. (**A–C**) Values for 13 control eyes. (**D–F**) Values for 18 carrier eyes. The *solid black horizontal bars* indicate the first and third quartiles. The *dashed horizontal black lines* represent the median values. The difference between the values for carrier and control eyes for the peripapillary locations **B** and **E** is statistically significant ($P < 0.05$, Welch's *t*-test).

myopic or had glaucoma or elevated eye pressure. The nature of peripapillary atrophy is not completely understood but among other causes could be related to choroidal deficiency due to obliteration of choriocapillaris as is suggested to occur in patients with glaucoma.[41,42] Choroidal degeneration has been shown following that of the RPE and photoreceptor complex in CHM.[17,43] Although, as a group, CHM carriers did not demonstrate decreased scotopic sensitivity in the majority of tested retinal locations, eyes individually exhibited a wide variance in DACP results, being in some cases (P1 OU, P4 OS, and P9 OS) consistently below the first quartile even within the carrier group. The decreased sensitivities are in accordance with results from the imaging modalities where the aforementioned patients had moderate to severe findings, such as interrupted EZ and ELM in SD-OCT, widespread reductions in autofluorescence, and below normal qAF values. An exception to this was P4 (OS) who presented with relatively large patches of normal autofluorescence in areas used to acquire qAF measurements. As a result, the calculated qAF value was within the lower limits of the 95% CI. On the other hand, P7 who had DACP results equal to or above the third quartile compared with both carrier and control groups, showed the least changes in imaging modalities. Based on these results, changes in visual function do not appear to precede findings in imaging modalities.

The X chromosome inactivation (lyonization) happens randomly in female subjects and results in cell populations expressing the mutant X chromosome intermingling with groups of cells expressing the normal X chromosome, creating a mosaic pattern in the fundus.[44,45] The degree of X-inactivation is variable and if it is skewed (75–90% of normal X chromosomes inactivated) symptoms of variable severity arise.[46] We interpret an underlying autofluorescence mosaicism in SW-AF and NIR-AF images as being a product of X-inactivation. This interpretation is based in part on features of SW-AF images acquired from GPR143/OA1 carriers wherein an RPE mosaicism in females presents as small-scaled, often rectangular, patches of darkness alternating with similar-sized foci of brightness.[24] In the CHM carriers examined here and in a previous study,[10] X-inactivation appears to create a mosaic of local differences in SW-AF and NIR-AF intensity. We suggest that the patches of lower AF in the mosaic observed here represent abnormal reductions in AF not due to variations in melanin optical density, as is the case for GPR143/OA1 carriers, but perhaps due to variations in the underlying densities of bisretinoid lipofuscin that are the source of the autofluorescence. Accordingly, reduced access to vitamin A leading to reduced bisretinoid formation could be an explanation for the patches of the mosaic having reduced SW-AF. In some but not all cases, patches of reduced AF in SW-AF images colocalized with reduced AF in NIR-AF images (see Fig 2, white rectangles).[10] We have observed in multiple studies[24,47,48] that the SW-AF signal can modulate the intensity of the NIR-AF. Thus, this relationship could account for the decrease in NIR-AF that parallels SW-AF reduction. One might have expected a reduction in vitamin A, if present, to also manifest as reduced rod sensitivity but this is not apparent from the current DACP findings perhaps because of insufficient resolution. With regard to the latter, the DAC perimeter uses a Goldmann size V test stimulus (1.73 degrees in diameter), and, in addition, the spacing between test locations ranged from 4 to 6 degrees. The sampling density may fail to detect patchy loss of rod function (i.e. areas containing rods with both mutant and normal X chromosome).

As also shown here, we have reported previously that qAF values are greatly decreased in CHM affected male subjects and female carriers.[10] The SW-AF measured by the qAF approach takes origin from the bisretinoid lipofuscin fluorophores that form in photoreceptor cells and accumulate in RPE. The formation of these fluorophores depends on vitamin A availability and is modulated by visual cycle kinetics. These fluorophores are also subject to photodegradation,[49,50] a process that also modulates fluorescence intensity. When photoreceptor cells have atrophied and no longer produce bisretinoid fluorophores, SW-AF intensity is reduced; SW-AF is also obliterated by RPE atrophy.[35,51] The latter process could readily be the explanation for the profound reduction in qAF observed in affected

patients with CHM.[10] Areas of atrophy in the carriers also contributed to appreciably reduced qAF values.

A variety of electrophysiologic and psychophysical tests have been used to assess visual function in CHM carriers under photopic, mesopic, or scotopic conditions. For example, full-field scotopic and photopic ERGs have been obtained from carriers in a number of studies and the majority have been found to be within normal limits. In a study by Sieving et al., 22 of 26 CHM carriers had normal full-field ERGs; they were normal for all 10 carriers in a study by Murro et al. and normal for 6 of 7 carriers in a study by Renner et al.[18–20] Compared to the full-field ERG that reflects a mass response of cones and rods of the entire retina to diffuse flashes of light, the multifocal ERG measures local cone mediated responses in the central retina.[52,53] The latter was used in a study by Vajaranant et al. and a mosaic pattern of retinal dysfunction was found in six out of seven CHM carriers, whereas only one subject demonstrated abnormal Humphrey VF thresholds.[54] The authors concluded that the multifocal ERG abnormalities corresponded to the severity of ophthalmoscopic pigmentary findings. Macular function has also been evaluated by microperimetry. For example, Thobani et al. described focal areas of threshold abnormalities in 50% of the CHM carriers, and Edwards et al. who assessed mean sensitivity values reported that they were reduced in all participants compared to normative data.[55,56] For both these studies, microperimetry was performed under mesopic conditions which may elicit cone and rod system mediated responses. One of the few studies that has investigated localized rod-mediated function in CHM carriers is by Mura et al.[40] Light and dark-adapted perimetry was used to determine whether a carriers' night vision complaints could be accounted for by the presence of patches of retinal dysfunction. Light-adapted "red/green" cone-mediated thresholds and 500 nm dark-adapted thresholds, obtained from a single carrier, were within normal limits, whereas 650 nm dark-adapted thresholds were markedly elevated at all test loci. The results were interpreted as reflecting impaired dark-adapted cone driven function.[40]

Pathophysiology in CHM carriers has not been thoroughly investigated and opposing views exist. Histopathological study of a CHM carrier donor eye found that the localization of the CHM gene product REP-1 was in rods but not cones[57] and microscopic examination of the photoreceptor layer revealed preferential loss of rods indicating rods as an initial location of degeneration.[18] Another histopathological study[12] concluded that the primary defect resides in the RPE. Studies of affected male patients often agree with notions of photoreceptors being the location of initial degeneration, but a recent study by Hagag et al. using a multimodal structure-function approach to investigate affected male patients suggests that vascular choroidal abnormalities precede photoreceptor loss in CHM.[58] Adaptive optics (AOs) has shown that cone photoreceptor densities are preserved in CHM carriers 2 to 8 degrees from the foveal center.[59] Although cone density is preserved, some retinal locations exhibit local regions of cone loss in AO images resulting in a patchy cone mosaic, these regions correspond to hypoautofluorescent locations in SW-AF and hyper-reflectivity in IR images.[60] Our findings demonstrating relatively normal scotopic sensitivity suggests that rod photoreceptor densities are also preserved.

One limitation of this study was a relatively small sample size of limited age range. Nevertheless, within this small cohort we captured varying stages of disease. Because this is a cross sectional study, we do not have any longitudinal data but, considering the slow progression rate of the condition, a long follow-up period would be required for meaningful findings. Additionally, for most subjects, we did not use a photopic test other than BCVA for visual function evaluation.

In conclusion, DACP provided valuable information regarding rod-mediated sensitivity in CHM carriers. In the majority of cases, rod sensitivity is preserved at levels that are comparable to those of healthy eyes in macular and peripheral areas. In the peripapillary area, statistically significant sensitivity loss was present. The findings appear to be accompanied by retinal changes observed on multimodal imaging. Further studies are needed to characterize scotopic vision and its alteration over time as it may prove useful for future trials looking to treat symptomatic CHM carriers.

Acknowledgments

Supported by grants from the National Eye Institute EY024091, P30EY019007, and EY009076; a grant from Research to Prevent Blindness to the Department of Ophthalmology, Columbia University; Jonas Children's Vision Care is supported by R01EY018213 and R01EY024698.

Disclosure: **R. Parmann**, None; **V.C. Greenstein**, None; **S.H. Tsang**, Abeona Therapeutics, Inc. (F), Emendo Bio, Inc. (F), Rejuvitas (O), Nanoscope Therapeutics (S); **J.R. Sparrow**, None

References

1. Zinkernagel MS, MacLaren RE. Recent advances and future prospects in choroideremia. *Clin Ophthalmol*. 2015;9:2195–1200.
2. Cremers FP, Sankila EM, Brunsmann F, et al. Deletions in patients with classical choroideremia vary in size from 45 kb to several megabases. *Am J Hum Genet*. 1990;47(4):622–628.
3. Simunovic MP, Jolly JK, Xue K, et al. The Spectrum of CHM Gene Mutations in Choroideremia and Their Relationship to Clinical Phenotype. *Invest Ophthalmol Vis Sci*. 2016;57(14):6033–6039.
4. McTaggart KE, Tran M, Mah DY, Lai SW, Nesslinger NJ, MacDonald IM. Mutational analysis of patients with the diagnosis of choroideremia. *Hum Mutat*. 2002;20(3):189–196.
5. Aleman TS, Han G, Serrano LW, et al. Natural History of the Central Structural Abnormalities in Choroideremia: A Prospective Cross-Sectional Study. *Ophthalmology*. 2017;124(3):359–373.
6. Jacobson SG, Cideciyan AV, Sumaroka A, et al. Remodeling of the human retina in choroideremia: rab escort protein 1 (REP-1) mutations. *Invest Ophthalmol Vis Sci*. 2006;47(9):4113–4120.
7. Roberts MF, Fishman GA, Roberts DK, et al. Retrospective, longitudinal, and cross sectional study of visual acuity impairment in choroideraemia. *Br J Ophthalmol*. 2002;86(6):658–662.
8. Huang AS, Kim LA, Fawzi AA. Clinical characteristics of a large choroideremia pedigree carrying a novel CHM mutation. *Arch Ophthalmol*. 2012;130(9):1184–1189.
9. Jolly JK, Xue K, Edwards TL, Groppe M, MacLaren RE. Characterizing the Natural History of Visual Function in Choroideremia Using Microperimetry and Multimodal Retinal Imaging. *Invest Ophthalmol Vis Sci*. 2017;58(12):5575–5583.

10. Paavo M, Carvalho JRL, Lee W, Sengillo JD, Tsang SH, Sparrow JR. Patterns and Intensities of Near-Infrared and Short-Wavelength Fundus Autofluorescence in Choroideremia Probands and Carriers. *Invest Ophthalmol Vis Sci*. 2019;60(12):3752–3761.
11. MacDonald IM, Russell L, Chan CC. Choroideremia: new findings from ocular pathology and review of recent literature. *Surv Ophthalmol*. 2009;54(3):401–407.
12. Flannery JG, Bird AC, Farber DB, Weleber RG, Bok D. A histopathologic study of a choroideremia carrier. *Invest Ophthalmol Vis Sci*. 1990;31(2):229–236.
13. Tolmachova T, Anders R, Abrink M, et al. Independent degeneration of photoreceptors and retinal pigment epithelium in conditional knockout mouse models of choroideremia. *J Clin Invest*. 2006;116(2):386–394.
14. Gordiyenko NV, Fariss RN, Zhi C, MacDonald IM. Silencing of the CHM gene alters phagocytic and secretory pathways in the retinal pigment epithelium. *Invest Ophthalmol Vis Sci*. 2010;51(2):1143–1150.
15. Preising M, Ayuso C. Rab escort protein 1 (REP1) in intracellular traffic: a functional and pathophysiological overview. *Ophthalmic Genet*. 2004;25(2):101–110.
16. MacDonald IM, Hume S, Zhai Y, Xu M. Choroideremia. In: Adam MP, Ardinger HH, Pagon RA , et al., eds. *GeneReviews*. University of Washington, Seattle Copyright 1993-2022, University of Washington, Seattle. GeneReviews is a registered trademark of the University of Washington, Seattle. All rights reserved; 1993.
17. Khan KN, Islam F, Moore AT, Michaelides M. Clinical and Genetic Features of Choroideremia in Childhood. *Ophthalmology*. 2016;123(10):2158–2165.
18. Sieving PA, Niffenegger JH, Berson EL. Electroretinographic findings in selected pedigrees with choroideremia. *Am J Ophthalmol*. 1986;101(3):361–367.
19. Murro V, Mucciolo DP, Passerini I, et al. Retinal dystrophy and subretinal drusenoid deposits in female choroideremia carriers. *Graefes Arch Clin Exp Ophthalmol*. 2017;255(11):2099–2111.
20. Renner AB, Kellner U, Cropp E, et al. Choroideremia: variability of clinical and electrophysiological characteristics and first report of a negative electroretinogram. *Ophthalmology*. 2006;113(11):2066.e1–2110.e1.
21. Preising MN, Wegscheider E, Friedburg C, Poloschek CM, Wabbels BK, Lorenz B. Fundus autofluorescence in carriers of choroideremia and correlation with electrophysiologic and psychophysical data. *Ophthalmology*. 2009;116(6):1201–1209.e1-2.
22. Renner AB, Fiebig BS, Cropp E, Weber BH, Kellner U. Progression of retinal pigment epithelial alterations during long-term follow-up in female carriers of choroideremia and report of a novel CHM mutation. *Arch Ophthalmol*. 2009;127(7):907–912.
23. Futter CE, Ramalho JS, Jaissle GB, Seeliger MW, Seabra MC. The role of Rab27a in the regulation of melanosome distribution within retinal pigment epithelial cells. *Mol Biol Cell*. 2004;15(5):2264–2275.
24. Paavo M, Zhao J, Kim HJ, et al. Mutations in GPR143/OA1 and ABCA4 Inform Interpretations of Short-Wavelength and Near-Infrared Fundus Autofluorescence. *Invest Ophthalmol Vis Sci*. 2018;59(6):2459–2469.
25. Zele AJ, Cao D. Vision under mesopic and scotopic illumination. *Front Psychol*. 2014;5:1594.
26. Lamb TD. Why rods and cones? *Eye (Lond)*. 2016;30(2):179–185.
27. McGuigan DB, Roman AJ, Cideciyan AV, et al. Automated Light- and Dark-Adapted Perimetry for Evaluating Retinitis Pigmentosa: Filling a Need to Accommodate Multicenter Clinical Trials. *Invest Ophthalmol Vis Sci*. 2016;57(7):3118–3128.
28. Bennett LD, Klein M, Locke KG, Kiser K, Birch DG. Dark-Adapted Chromatic Perimetry for Measuring Rod Visual Fields in Patients with Retinitis Pigmentosa. *Transl Vis Sci Technol*. 2017;6(4):15.
29. Pfau M, Lindner M, Müller PL, et al. Effective Dynamic Range and Retest Reliability of Dark-Adapted Two-Color Fundus-Controlled Perimetry in Patients With Macular Diseases. *Invest Ophthalmol Vis Sci*. 2017;58(6):BIO158–BIO167.
30. Delori F, Greenberg JP, Woods RL, et al. Quantitative measurements of autofluorescence with the scanning laser ophthalmoscope. Comparative Study Research Support, N.I.H., Extramural Research Support, Non-U.S. Gov't. *Invest Ophthalmol Vis Sci*. 2011;52(13):9379–9390.
31. Burke TR, Duncker T, Woods RL, et al. Quantitative fundus autofluorescence in recessive Stargardt disease. *Invest Ophthalmol Vis Sci*. 2014;55(5):2841–2852.
32. Duncker T, Greenberg JP, Ramachandran R, et al. Quantitative fundus autofluorescence and optical coherence tomography in Best vitelliform macular dystrophy. Research Support, N.I.H., Extramural Research Support, Non-U.S. Gov't. *Invest Ophthalmol Vis Sci*. 2014;55(3):1471–1482.
33. Duncker T, Tsang SH, Lee W, et al. Quantitative fundus autofluorescence distinguishes ABCA4-associated and non-ABCA4-associated bull's-eye maculopathy. *Ophthalmology*. 2015;122(2):345–355.
34. Sparrow JR, Duncker T, Woods R, Delori FC. Quantitative Fundus Autofluorescence in Best Vitelliform Macular Dystrophy: RPE Lipofuscin is not Increased in Non-Lesion Areas of Retina. *Adv Exp Med Biol*. 2016;854:285–290.
35. Greenberg JP, Duncker T, Woods RL, Smith RT, Sparrow JR, Delori FC. Quantitative fundus autofluorescence in healthy eyes. *Invest Ophthalmol Vis Sci*. 2013;54(8):5684–5693.
36. Ba-Abbad R, Sergouniotis PI, Plagnol V, et al. Clinical characteristics of early retinal disease due to CDHR1 mutation. *Mol Vis*. 2013;19:2250–2259.
37. Stingl K, Mayer AK, Llavona P, et al. CDHR1 mutations in retinal dystrophies. *Sci Rep*. 2017;7(1):6992.
38. Tan RS, Guymer RH, Aung KZ, Caruso E, Luu CD. Longitudinal Assessment of Rod Function in Intermediate Age-Related Macular Degeneration With and Without Reticular Pseudodrusen. *Invest Ophthalmol Vis Sci*. 2019;60(5):1511–1518.
39. Bennett LD, Metz G, Klein M, Locke KG, Khwaja A, Birch DG. Regional Variations and Intra-/Intersession Repeatability for Scotopic Sensitivity in Normal Controls and Patients With Inherited Retinal Degenerations. *Invest Ophthalmol Vis Sci*. 2019;60(4):1122–1131.
40. Mura M, Sereda C, Jablonski MM, MacDonald IM, Iannaccone A. Clinical and functional findings in choroideremia due to complete deletion of the CHM gene. *Arch Ophthalmol*. 2007;125(8):1107–1113.
41. Hayreh SS. Blood supply of the optic nerve head and its role in optic atrophy, glaucoma, and oedema of the optic disc. *Br J Ophthalmol*. 1969;53(11):721–748.
42. Fantes FE, Anderson DR. Clinical histologic correlation of human peripapillary anatomy. *Ophthalmology*. 1989;96(1):20–25.
43. Jain N, Jia Y, Gao SS, et al. Optical Coherence Tomography Angiography in Choroideremia: Correlating Choriocapillaris Loss With Overlying Degeneration. *JAMA Ophthalmol*. 2016;134(6):697–702.
44. Lyon MF. X-chromosome inactivation and human genetic disease. *Acta Paediatr Suppl*. 2002;91(439):107–112.
45. Fahim AT, Daiger SP. The Role of X-Chromosome Inactivation in Retinal Development and Disease. *Adv Exp Med Biol*. 2016;854:325–331.

Investigative Ophthalmology & Visual Science

46. Wuthisiri W, Lingao MD, Capasso JE, Levin AV. Lyonization in ophthalmology. *Curr Opin Ophthalmol*. 2013;24(5):389–397.
47. Duncker T, Lee W, Tsang SH, et al. Distinct characteristics of inferonasal fundus autofluorescence patterns in Stargardt disease and retinitis pigmentosa. Comparative Study Research Support, N.I.H., Extramural Research Support, Non-U.S. Gov't. *Invest Ophthalmol Vis Sci*. 2013;54(10):6820–6826.
48. Duncker T, Tabacaru MR, Lee W, Tsang SH, Sparrow JR, Greenstein VC. Comparison of near-infrared and short-wavelength autofluorescence in retinitis pigmentosa. *Invest Ophthalmol Vis Sci*. 2013;54(1):585–591.
49. Ueda K, Zhao J, Kim HJ, Sparrow JR. Photodegradation of retinal bisretinoids in mouse models and implications for macular degeneration. *Proc Natl Acad Sci USA*. 2016;113(25):6904–6909.
50. Ueda K, Kim HJ, Zhao J, Sparrow JR. Bisretinoid Photodegradation Is Likely Not a Good Thing. *Adv Exp Med Biol*. 2018;1074:395–401.
51. Paavo M, Lee W, Allikmets R, Tsang S, Sparrow JR. Photoreceptor cells as a source of fundus autofluorescence in recessive Stargardt disease. *J Neurosci Res*. 2019;97(1):98–106.
52. Robson AG, Nilsson J, Li S, et al. ISCEV guide to visual electrodiagnostic procedures. *Doc Ophthalmol*. 2018;136(1):1–26.
53. Tsang SH, Sharma T. Electroretinography. *Adv Exp Med Biol*. 2018;1085:17–20.
54. Vajaranant TS, Fishman GA, Szlyk JP, Grant-Jordan P, Lindeman M, Seiple W. Detection of mosaic retinal dysfunction in choroideremia carriers electroretinographic and psychophysical testing. *Ophthalmology*. 2008;115(4):723–729.
55. Thobani A, Anastasakis A, Fishman GA. Microperimetry and OCT findings in female carriers of choroideremia. *Ophthalmic Genet*. 2010;31(4):235–239.
56. Edwards TL, Groppe M, Jolly JK, Downes SM, MacLaren RE. Correlation of retinal structure and function in choroideremia carriers. *Ophthalmology*. 2015;122(6):1274–1276.
57. Syed N, Smith JE, John SK, Seabra MC, Aguirre GD, Milam AH. Evaluation of retinal photoreceptors and pigment epithelium in a female carrier of choroideremia. *Ophthalmology*. 2001;108(4):711–720.
58. Hagag AM, Mitsios A, Narayan A, et al. Prospective deep phenotyping of choroideremia patients using multimodal structure-function approaches. *Eye (Lond)*. 2021;35(3):838–852.
59. Suzuki K, Gocho K, Akeo K, et al. High-Resolution Retinal Imaging Reveals Preserved Cone Photoreceptor Density and Choroidal Thickness in Female Carriers of Choroideremia. *Ophthalmic Surg Lasers Imaging Retina*. 2019;50(2):76–85.
60. Morgan JI, Han G, Klinman E, et al. High-resolution adaptive optics retinal imaging of cellular structure in choroideremia. *Invest Ophthalmol Vis Sci*. 2014;55(10):6381–6397.

Investigative Ophthalmology & Visual Science